Global contributions of mesoscale dynamics to meridional heat transport

Andrew Delman[1] and Tong Lee[1]

[1]Jet Propulsion Laboratory, California Institute of Technology, Pasadena, CA, USA

Correspondence: Andrew Delman (adelman@jpl.caltech.edu)

Abstract.

Mesoscale ocean processes are prevalent in many parts of the global oceans, and may contribute substantially to the meridional movement of heat. Yet earlier global surveys of meridional heat transport (MHT) have not formally distinguished between mesoscale and large-scale contributions, or have defined eddy contributions based on temporal rather than spatial characteristics. This work uses spatial filtering methods to separate large-scale (gyre and planetary wave) contributions from mesoscale (eddy, recirculation, and tropical instability wave) contributions to MHT by extending beyond a previous effort for the North Atlantic Ocean. Overall, mesoscale temperature fluxes produce a net poleward MHT at mid-latitudes and equatorward MHT in the tropics, thereby resulting in a net divergence of heat from the subtropics. Mesoscale temperature fluxes are often concentrated near the energetic currents at western boundaries, and the temperature difference between the boundary current and its recirculation determines the direction of the mesoscale temperature flux. The mesoscale contribution to MHT yields substantially different results from temporally-based "eddy" contributions to MHT, with the latter contributed substantially by gyre and planetary wave motions at low latitudes. Mesoscale temperature fluxes contribute the most to interannual and decadal variability of MHT in the Southern Ocean, the tropical Indo-Pacific, and the North Atlantic. Surface eddy kinetic energy (EKE) is not a good proxy for mesoscale temperature flux variability in regions with the highest time-mean EKE, though it does explain much of the temperature flux variability in regions of modest time-mean EKE. This approach to quantifying mesoscale fluxes can be used to improve parameterizations of mesoscale effects in coarse-resolution models, and assess regional impacts of mesoscale eddies and recirculations on tracer fluxes.

1 Introduction

Along frontal gradients in the ocean, instabilities form that exchange waters of different temperatures, resulting in heat transport across latitude lines. Many of these instabilities (eddies) assume scales comparable to or slightly larger than the baroclinic radius of deformation (e.g., Chelton et al., 2011), corresponding to the oceanic mesoscale (tens to hundreds of kilometers). In addition to eddies, tropical instability waves (TIWs; e.g., Jochum and Murtugudde, 2006) and recirculation gyres that flank

boundary current jets also have the capacity to move heat meridionally in the ocean at mesoscales. Unlike the wind-forced

25   response associated with larger-scale gyres and planetary waves, these mesoscale phenomena are generated and sustained by nonlinear mechanisms such as baroclinic and barotropic instability (e.g., Eady, 1949; Charney and Stern, 1962) and nonlinear momentum advection (e.g., Greatbatch et al., 2010).

Despite the prevalence of mesoscale features in the global oceans, relatively little attention has been given to quantifying their contributions to meridional heat transport (MHT) until recently. Most of the literature characterizing the oceanic MHT

30   emphasizes the dominant role of the overturning circulation (e.g., Talley, 2003), arising from the steep vertical temperature gradients at lower latitudes. Some of these studies assess the "gyre" contribution separately from the overturning (e.g., Bryan, 1982; Johns et al., 2011). In this framework, the overturning contribution is the integrated product of the zonal mean meridional velocity v and temperature T, and the gyre contribution consists of the residual (zonally-varying) v and T. However, no distinction is made between the temperature flux associated with the basin-scale gyres vs. smaller mesoscale processes. This

35   distinction is important not only because the forcing mechanisms for basin-scale motions are quite different from mesoscale motions, but also because the coarse-resolution oceans in most climate model simulations do not explicitly represent mesoscale motions and must parameterize their effects. In recent years, eddy tracking and identification methods (e.g., Chaigneau and Pizarro, 2005; Chelton et al., 2011; Laxenaire et al., 2018) have been used to quantify the specific MHT or temperature flux contributions of identified eddies (e.g., Hausmann and Czaja, 2012; Dong et al., 2014, 2017; Sun et al., 2019; Müller et al.,

40   2019; Laxenaire et al., 2020). Yet not all mesoscale flow features take the form of coherent vortices, and the actual movement of coherent eddies likely accounts for a relatively small portion of the fluxes associated with the mesoscale (e.g., Hausmann and Czaja, 2012; Abernathey and Haller, 2018).

Another commonly-used approach is to quantify the "eddy" contribution to MHT based on the deviation of v and T from the temporal (rather than zonal) mean (e.g., Cox, 1985; Jayne and Marotzke, 2002; Griffies et al., 2015; Ushakov and Ibrayev,

45   2018). Jayne and Marotzke (2002) used this formulation to assess eddy temperature fluxes and MHT, finding eddy temperature fluxes in energetic mid-latitude regions (Antarctic Circumpolar Current, western boundary current extensions) that are consistent with downgradient diffusivity estimates (e.g., Stammer, 1998). Volkov et al. (2008) defined the eddy contribution as the deviation from 3-month means of v and T, hence their high-frequency eddy contribution to MHT was somewhat lower than the total time-varying contribution quantified by Jayne and Marotzke (2002). Yet these temporal decomposition methods may

50   conflate the contributions of large-scale and mesoscale circulations, as gyres and planetary waves have temporal covariances between v and T. Moreover, the effects of stationary mesoscale features (e.g., recirculation gyres) are not included in the temporal eddy MHT contributions, even though it is important to quantify these effects in order to assess coarse-resolution model parameterizations of mesoscale fluxes.

This study extends the methodology that Delman and Lee (2020) used in the North Atlantic, in order to better understand

55   the specific contribution of mesoscale processes to meridional temperature fluxes and MHT globally. Three focus areas of this study are to: (1) assess time-mean and interannual/decadal variability of mesoscale MHT relative to the overturning and large-scale circulations, (2) compare the mesoscale MHT to other "eddy" MHT diagnostics, and (3) determine the extent to which surface eddy kinetic energy (EKE) can be used as a proxy for the variability of mesoscale temperature fluxes that contribute to

MHT. Section 2 briefly discusses the ocean general circulation model and methods used to quantify the components of MHT. Section 3 quantifies the components of MHT globally and maps the distribution of the mesoscale temperature flux (MTF). Section 4 compares the integrated mesoscale MHT contributions to temporally-based measures of the eddy MHT. Section 5 assesses the global distribution of the interannual and decadal variability of the MTF and its relationship with surface EKE variability. Section 6 discusses the key conclusions of this study and identifies areas in need of future investigation.

2 Methods

2.1 Model simulation and validation of EKE

To quantify mesoscale temperature fluxes and contributions to MHT, this analysis uses output from an eddy-permitting ocean general circulation model, the Parallel Ocean Program (POP) 2 (Smith et al., 2010). POP integrates the primitive equations with a z-depth coordinate, and is configured in a tripole grid with two north poles over Canada and Siberia. The simulation was run on the Yellowstone computing cluster (Computational and Information Systems Laboratory, 2016), with a 0.1° longitude grid spacing in the Mercator portion of the grid south of ∼28°N, and progressively finer grid spacing approaching the two north poles. The ocean surface is forced with Coordinated Ocean-Ice Reference Experiments version 2 (COREv2; Large and Yeager, 2009) fluxes based on National Centers for Environmental Prediction reanalysis with corrections from satellite data. The simulation was spun up during a 15-year period forced by CORE normal-year forcing (Large and Yeager, 2004), followed by a 33-year model integration with COREv2 interannually-varying fluxes corresponding to the years 1977–2009. Our analysis covers the 32-year period 1978–2009, the same span of time as in Delman and Lee (2020). For more details of the model simulation see Johnson et al. (2016) and Delman et al. (2018).

As a proxy for the model's representation of mesoscale activity globally, the model time-mean surface EKE was compared with surface EKE from altimetry data. The altimetry dataset used is produced by Collecte Localisation Satellites (Ducet et al., 2000) and made available through the Copernicus Marine Environment Monitoring Service (CMEMS), with data merged from numerous altimetry missions onto a grid at 1/4° spatial and daily temporal resolution. The analysis demonstrates that the locations and EKE levels of the most energetic regions of the ocean are well represented in the POP simulation (Figure 1). However, it is also important to note that POP underrepresents EKE in many other regions of the ocean; including the subtropical eddy bands between 15° and 30° latitude in the North and South Pacific and South Indian Oceans, and to a lesser extent the TIW region near the equator. Therefore, our estimates of mesoscale temperature fluxes in subtropical and tropical regions are likely to be underestimates of the true fluxes.

2.2 Computing the mesoscale temperature flux

As in Delman and Lee (2020), this study decomposes meridional temperature fluxes into three components (overturning, large-scale, and mesoscale) by applying spatial filters to zonal profiles of meridional velocity v and temperature T. The meridional temperature transport is related to MHT by a factor of ρc_ρ, where ρ is the density and c_ρ the specific heat capacity of seawater.
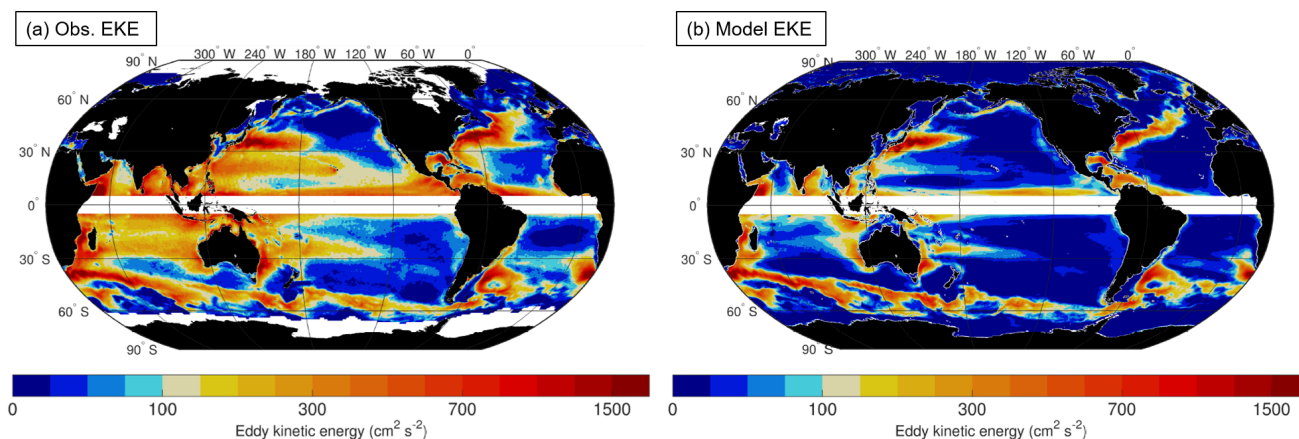
Figure 1. Time mean surface eddy kinetic energy (EKE), from (a) the Copernicus Marine Environment Monitoring Service (CMEMS) satellite-based gridded product, and (b) the POP model, with wavelengths <0.5° filtered out. Time averages were computed 1993–2016 from the satellite data and the years corresponding to 1978–2009 in the model simulation. Regions within 5° latitude of the equator are masked out.

90 Integrated across an ocean basin, the meridional temperature flux can be decomposed into zonal mean and zonal deviation components

$$\int vT \, dx = \int \left(\langle v \rangle \langle T \rangle + v'' T'' \right) dx \tag{1}$$

where $\langle \rangle$ indicates the zonal mean and $''$ indicates the deviation from the zonal mean. The first term on the right-hand side $\langle v \rangle \langle T \rangle$ is the overturning component of the meridional temperature flux, consistent with earlier studies (e.g., Bryan, 1982;

95 Johns et al., 2011). The overturning component, when multiplied by ρc_ρ and zonally integrated, gives the portion of MHT associated with basin-wide vertical gradients in meridional flow and temperature. The second term, variously referred to as the gyre or eddy temperature flux, contains all contributions from horizontally-varying v and T. Our method further decomposes this term into contributions from large-scale and mesoscale variations in v and T

$$v'' = v_L + v_M \tag{2}$$

100

$$T'' = T_L + T_M \tag{3}$$

$$v'' T'' = v_L T_L + \left[(v_L T_M + v_M T_L) + v_M T_M \right] \tag{4}$$

The first term on the right-hand side is the contribution from the large-scale circulation, while the remaining three terms consti-
105 tute the mesoscale temperature flux (MTF). The cross terms $v_L T_M + v_M T_L$ are considered part of the mesoscale contribution
since these fluxes would not exist without mesoscale structures. In practice, $v_L T_M$ is generally negligible compared to the
other terms since zonal T profiles are red-shifted (have more large-scale structure) compared to zonal v profiles. However,
$v_M T_L$ can be the largest contributor to the MTF, especially near boundaries where large-scale temperature deviations from the
zonal mean are often substantial.

110 The spatial filters to compute the large-scale and mesoscale v and T are applied in the zonal wavenumber domain, with v
weighted by Δx (the length of each grid face along the transect) to better conserve volume transport across the transect. The
Fourier coefficients $V(k)$ of $v\Delta x$ and T are filtered according to the transfer functions

$$V_L(k) = \left[0.5 + 0.5\mathrm{erf}\left(-s\,ln\frac{|k|}{k_0}\right)\right]V(k) \tag{5}$$

$$V_M(k) = \left[0.5 + 0.5\mathrm{erf}\left(s\,ln\frac{|k|}{k_0}\right)\right]V(k) \tag{6}$$

with s the steepness factor (set to 5) and k_0 the threshold wavenumber for separating the large-scale and mesoscale. Accor-
dingly, $\lambda_0 = 1/k_0$ is the threshold wavelength for the scale separation between large-scale and mesoscale.

A zonal spatial filter was used to separate large-scale and mesoscale MHT contributions in Zhao et al. (2018); in addition
to using a different filter, our method incorporates boundary and channel corrections (described in detail in Delman and Lee,
120 2020) to better preserve zero net volume/mass flux in the basin-integrated v_L and v_M components. One aspect of note is that in
channels bounded by bathymetry, where the width of the channel is narrower than $\lambda_0/4$, the meridional velocity components
are set to $v_L = v$ and $v_M = 0$. This is because the channel is too narrow for a meaningful large-scale/mesoscale separation,
and the basin-wide volume and mass transport is better conserved in the large-scale component when the channel transport is
included in the large-scale circulation (e.g., the Gulf Stream in the Florida Strait).

125 2.3 Mesoscale transition scale

Delman and Lee (2020) used $\lambda_0 = 10°$ longitude as the threshold wavelength in the North Atlantic, based on spectral analyses
of meridional velocity and temperature at a range of latitudes. For this study, similar spectral analyses were carried out in
the Atlantic, Indo-Pacific, and Southern ocean basins; the meridional velocity spectra are shown at various latitudes in the
Indo-Pacific and Southern ocean basins as examples (Figure 2). As in Delman and Lee (2020), the mesoscale/large-scale
130 transition and mesoscale peak wavelengths were estimated from each transect based on the logarithmically-smoothed spectral
density profiles. The choice of $\lambda_0 = 10°$ longitude was found to be reasonable at and poleward of 20° latitude. Even where
the objectively-identified transition wavelength was very different from 10° (e.g., 20°S in the Indo-Pacific as shown in Fig.
2e), the mesoscale "bump" in the spectra clearly occurs at scales smaller than 10°. The one exception to this pattern is at some

tropical latitudes (e.g., 10°S Indo-Pacific, Fig. 2d), where the mesoscale bump extends to scales larger than 10° longitude.

135 Given this, and the abrupt growth of the deformation radius and typical eddy scales equatorward of 20° (Chelton et al., 2011), the transition wavelength was set to $\lambda_0 = 20°$ longitude within 10° of the equator, $\lambda_0 = 10°$ poleward of 20° latitude in both hemispheres, with a linear transition in λ_0 in the 10°–20° latitude range.
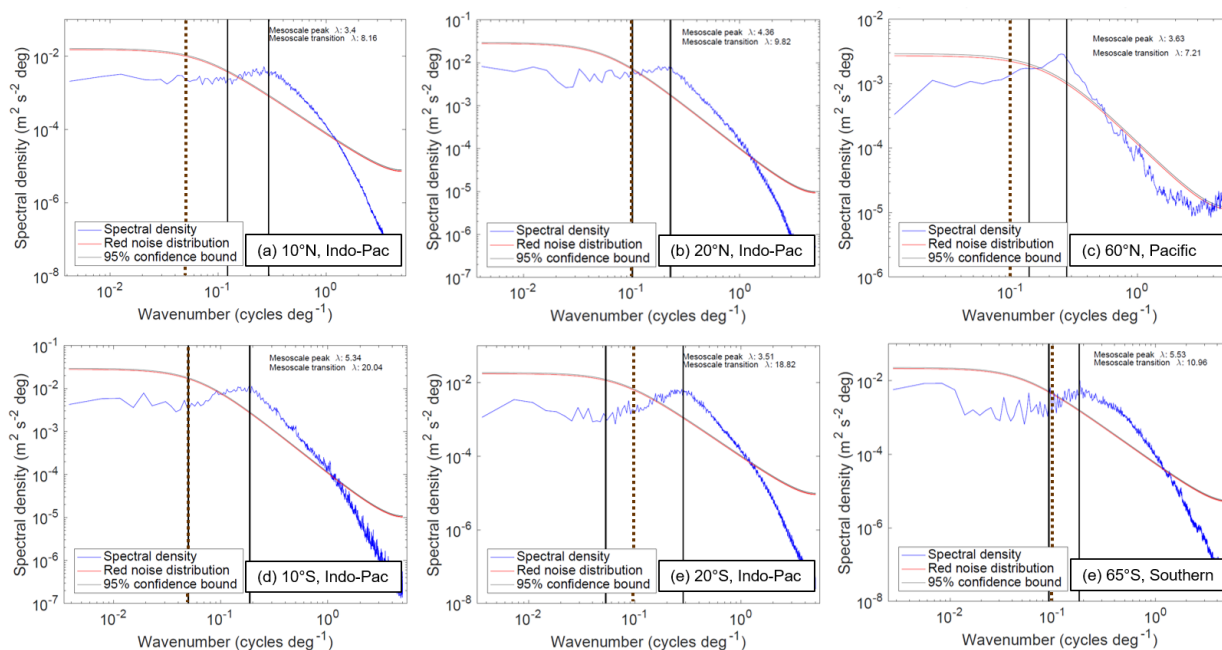
Figure 2. Zonal wavenumber spectral density of meridional velocity in POP, along latitude transects in specified basins. The black vertical lines and small text indicate the wavelength associated with the mesoscale transition and peak, as computed using the logarithmically-smoothed spectral density profile. The vertical dashed brown line indicates the wavelength λ_0 chosen for the mesoscalelarge-scale threshold at that latitude. The red and gray curves indicate the red noise distribution expected from lag-1 (model grid-scale) autocorrelation and the corresponding 95% confidence bound.

3 Global distribution of heat transport components and temperature fluxes

3.1 Barotropic flow streamfunction

140 To place the global distribution of temperature fluxes in the context of the large-scale flow field in POP, the time-mean cumulative zonal integral of the volume transport in each basin is shown (Figure 3). This integral is equivalent to the barotropic streamfunction, except that the circumpolar transport in the Southern Ocean is not included. The major gyre circulations are all visible in these maps; these include (1) cyclonic tropical gyres between ∼0°-15° latitude in all basins except the northern

Indian Ocean where the time-mean flow is weak, (2) subtropical gyres spanning ~15°-40° latitude, except in the Southern

145   Hemisphere where these gyres are partially connected by the Antarctic Circumpolar Current (ACC), and (3) subpolar gyres in

the north Atlantic and Pacific, with the Southern Ocean dominated by the meridional drift in the ACC.
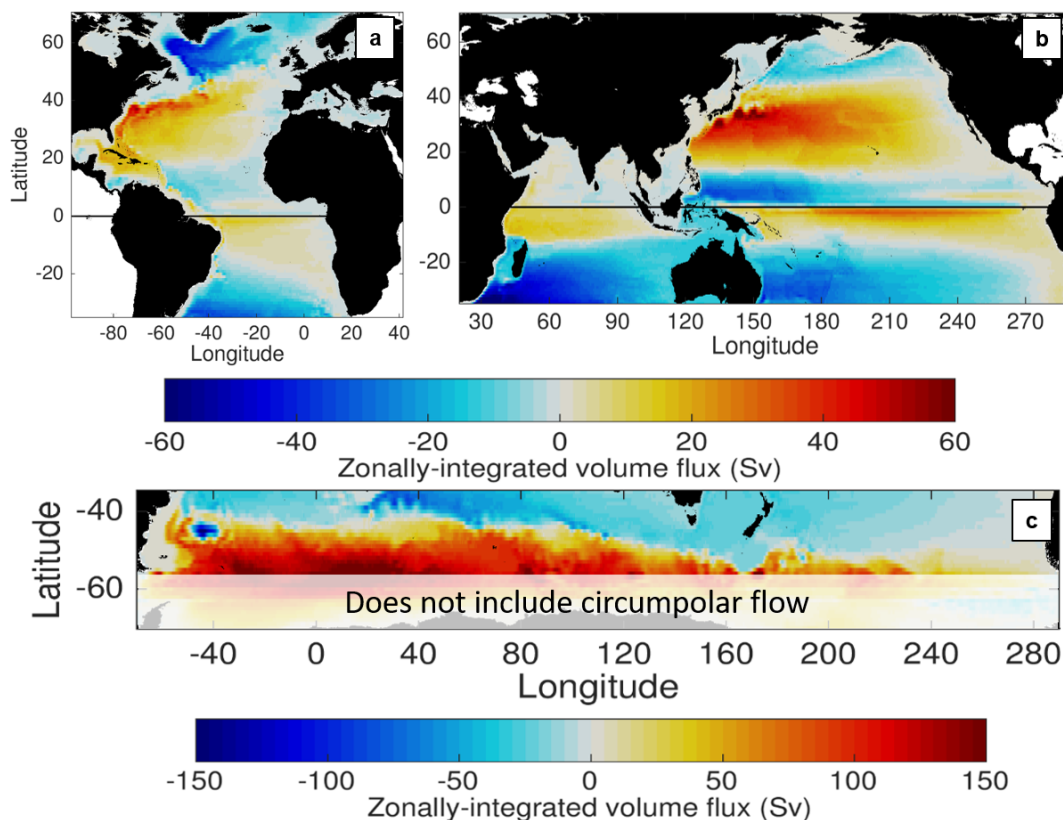
Figure 3. POP time mean (1978–2009) cumulative zonally-integrated volume flux in the (a) Atlantic, (b) Indo-Pacific, and (c) Southern Ocean basins. This is equivalent to the barotropic streamfunction in each basin, except panel (c) does not include the Drake Passage volume transport; the latitudes south of Cape Horn are faded to indicate this.

3.2   Spatial components of meridional heat transport

When integrated zonally within ocean basins or across the global ocean, the contribution of the mesoscale temperature flux (MTF) to time-mean MHT is largest at mid-latitudes, with substantial contributions in the Indo-Pacific tropics as well (Figure

150   4). The largest magnitude mesoscale contribution to MHT at any latitude is at 40°S, with a poleward heat transport (-0.6 PW). This exceeds the contribution of the large-scale MHT and nearly counters the equatorward MHT (0.8 PW) associated with the overturning at that latitude. The Northern Hemisphere mid-latitude MHT contributions are not as large; however, the
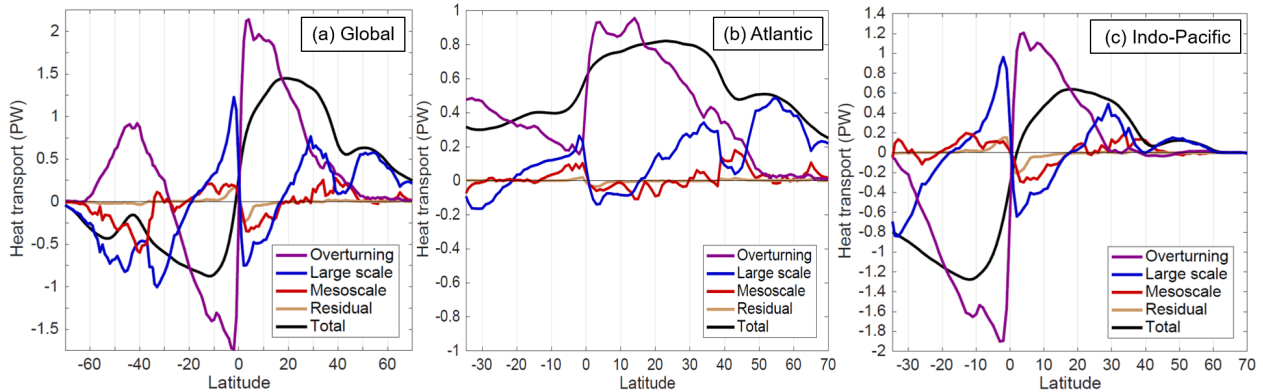
Figure 4. Spatial decomposition of the time mean meridional heat transport as a function of latitude (a) globally, and in the (b) Atlantic and (c) Indo-Pacific. Positive values indicate a northward heat transport.

mesoscale MHT contribution in the North Atlantic at 43°–45°N is almost comparable to the overturning at those latitudes (in this case both components are poleward). In the North Pacific, the mesoscale contributes to poleward MHT at ~35°-

155   42°N where the overturning and large-scale contributions essentially vanish. Both the Southern and Northern Hemisphere mid-latitude peaks in mesoscale MHT coincide with local minima in the magnitude of the large-scale MHT (Figure 4a). This suggests that the mesoscale plays an important part in conveying poleward MHT from the subtropical to subpolar gyres in the Northern Hemisphere, and across the subtropical edges of the Southern Ocean. Additional notable mesoscale contributions to time-mean MHT are found at the Indo-Pacific at 2°-9°N (~0.3 PW) and at 15°-11°S (~0.2 PW).
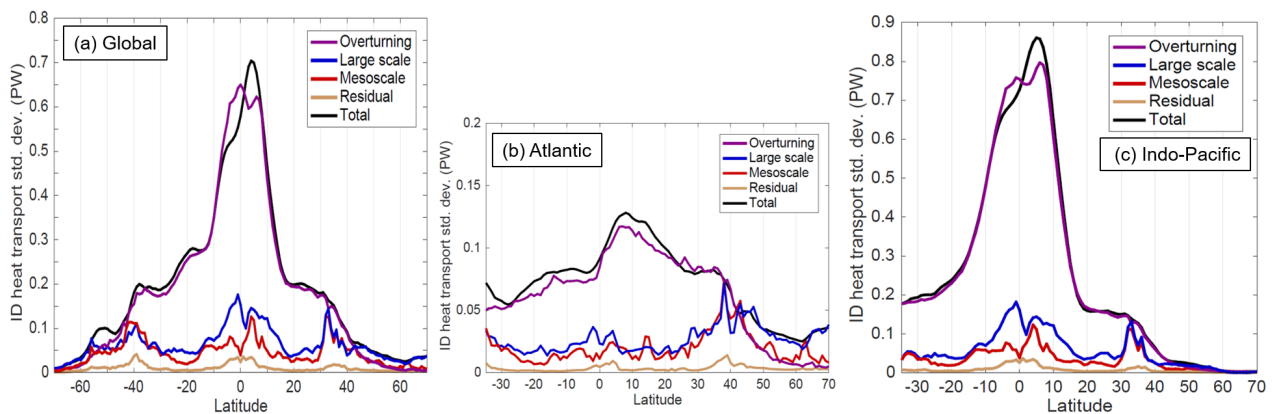
Figure 5. Interannual/decadal (ID) standard deviation of the spatial components of meridional heat transport (a) globally and in the (b) Atlantic and (c) Indo-Pacific basins. The ID time series of each component of MHT have been low-passed for periods longer than 14 months, with the seasonal cycle explicitly removed.

160   A key focus of this study is a better understanding of the interannual/decadal (ID) variability of the mesoscale contribution to MHT; accordingly the time series of the spatial components at each latitude have been temporally low-passed for periods >14 months and the seasonal cycle explicitly removed. The standard deviations of the ID filtered components (Figure 5) show that the overturning dominates MHT variability at most latitudes, but that mesoscale MHT variability can be comparable to the overturning and large-scale contributions at mid and high latitudes. Globally, the amplitude of mesoscale MHT variability at

165   ID timescales is generally comparable to the large-scale variability poleward of 30° latitude, and comparable to the overturning variability poleward of 40° latitude in both hemispheres (Figure 5a). The largest peaks in ID mesoscale MHT variability occur at 43°–40°S, 3°–4°N, and 32°N, with the latter two peaks explained mostly by contributions from the Indo-Pacific (Figure 5c).

In order to understand the mechanisms for the time-mean and time-variable contributions of the spatial components to MHT, we consider the spatial distribution of temperature fluxes within each ocean basin. The overturning flux is by definition spatially

170   uniform along a given transect and depth level, so we focus attention on the distribution of the large-scale temperature flux (LTF) and the MTF. One important caveat is that the LTF and MTF defined in equation (4) each consist of rotational and divergent fluxes (Marshall and Shutts, 1981); by definition, the rotational temperature (and heat) fluxes do not contribute to changes in ocean temperature or heat content and therefore are not generally of interest for climate studies. Our decomposition method is applied only in one horizontal dimension (zonally) so the divergent flux can not be neatly separated from the

175   rotational flux except in basin integrals (where the rotational flux is negligible). However, Jayne and Marotzke (2002) showed that rotational fluxes in mesoscale-active areas also take on mesoscale structure (i.e., they recirculate at mesoscales), while divergent meridional fluxes tend to have larger-scale structure particularly in the zonal direction. Hence, in this study a zonal smoothing filter is applied to maps of temperature fluxes to reduce contamination from the "noise" of the rotational fluxes. This smoothing filter has the same form as the low-pass filter in equation (5), but with $s = 2$ and the threshold wavenumber k_0 equal to

180   half the threshold wavenumber (twice the threshold wavelength) for the large-scale/mesoscale separation at that latitude. Thus the mapped LTF and MTF both have large-scale structure; the smoothed MTF indicates the effect of the mesoscale circulation rectified to larger scales, with its mesoscale structure (mostly rotational fluxes) removed. It is the impact of mesoscale fluxes on large-scale temperature distributions that is most relevant when quantifying the fluxes that need to be parameterized in coarse-resolution models.

185   Global maps of zonally-smoothed time-mean LTF (Figure 6) show structural patterns that generally correspond to the position of the major oceanic gyres. Within 15° of the equator, LTFs are fairly consistently towards the equator (positive south of the equator and negative to the north). These equatorward temperature fluxes associated with the horizontal circulation are in opposition to the poleward fluxes of the vertical overturning circulation at these latitudes (Figure 4), while their consistency suggests that both the western and eastern sides of the ocean basins contribute significantly to the large-scale equatorward

190   MHT. At the latitudes of the subtropical gyres (∼15°-40° latitude) the LTF generally has three distinct regions: strongly poleward in the vicinity of the western boundary, weakly equatorward in the interior western half, and weakly poleward in the eastern half of the basin. This pattern can be attributed to the asymmetry in the meridional flow; the poleward flow is concentrated very close to the western boundary (Figure 3), while the temperature profile in the upper ocean (warmer in the west, cooler in the east) changes more gradually. Hence the equatorward temperature flux results from equatorward (generally Sverdrup
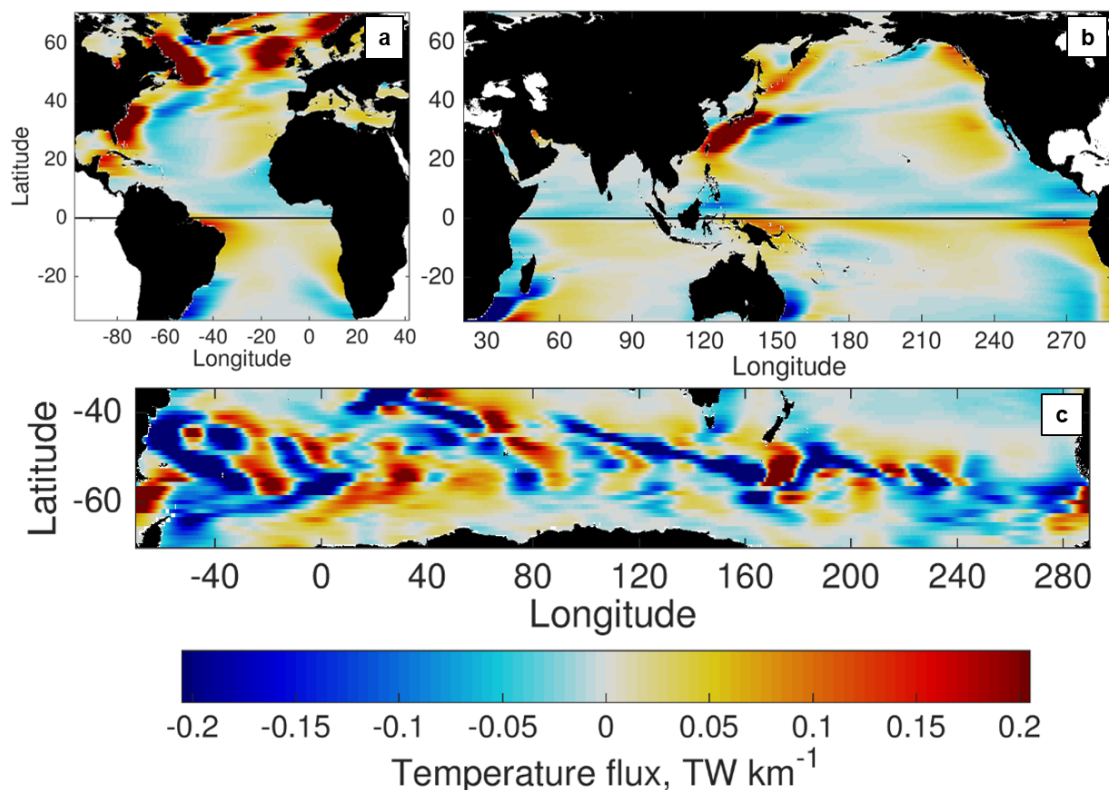
Figure 6. POP time-mean northward temperature flux associated with the large-scale flow (LTF), in units of terawatts per kilometer (TW km^{-1}), zonally low-passed using a wavelength equal to twice the large-scale/mesoscale threshold wavelength at each latitude. Fluxes shown in the (a) Atlantic, (b) Indo-Pacific, and (c) Southern Ocean basins.

195   flow) in the warmer part of the basin. Nonetheless, the strongest contribution from the large-scale subtropical gyre is poleward, at the western boundary. This picture becomes more complex in the Northern Hemisphere subpolar gyres (Fig. 6a,b) and the Southern Ocean (Fig. 6c). In the subpolar gyres, poleward temperature fluxes are substantial near both western and eastern boundaries. In the Southern Ocean, poleward (negative) temperature fluxes are most substantial where there are meridional excursions in the ACC, such as east of South America (60°-30°W), south of Australia (100°-160°E), and before the entrance

200   to Drake Passage (240°-280°E).

     Maps of zonally-smoothed time-mean MTF (Figure 7) show that the mesoscale contributions to MHT are generally concentrated near the western boundary, even more so than LTF contributions. Even in the tropics, MTF contributions are mostly confined to the western boundaries, with the exception of the TIW band in the north-central equatorial Pacific, and to a lesser extent in the eddy-rich region south of Indonesia. As Figure 4 implies, the impact of both LTF and MTF contributions to MHT

205   is generally to flux heat equatorward in the tropics, and poleward at higher latitudes. Consistent with this, the time-mean me-
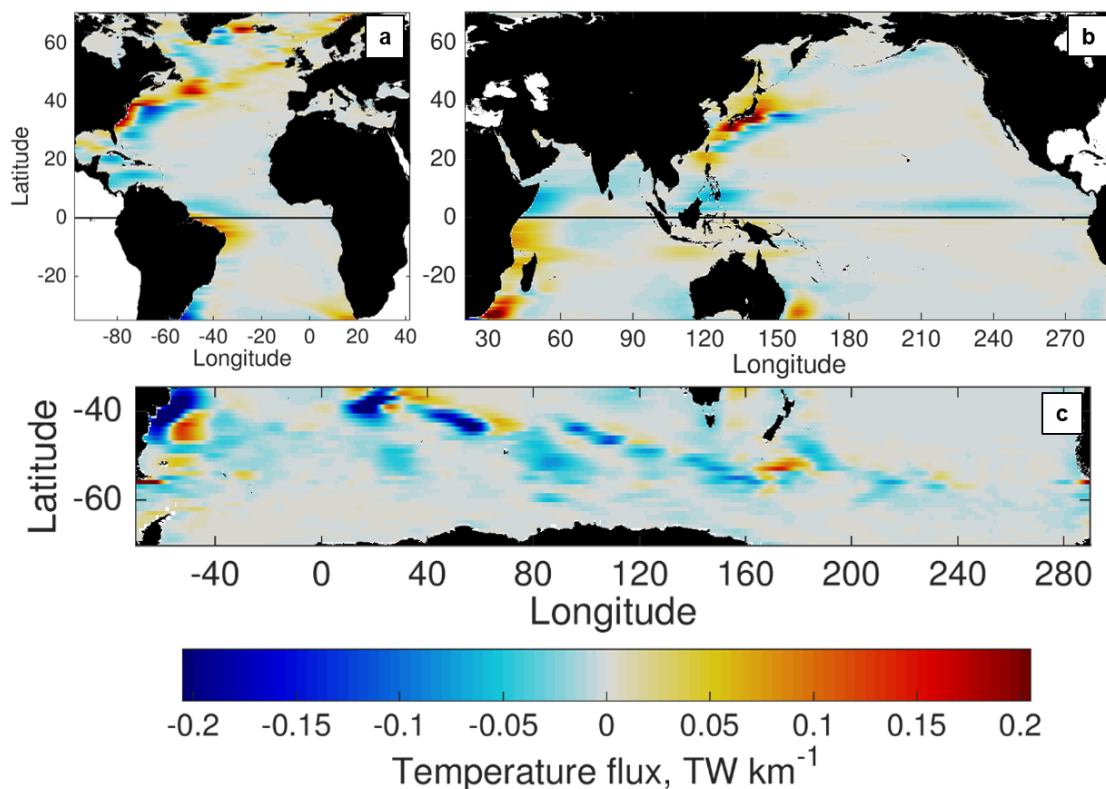
Figure 7. POP time-mean northward temperature flux associated with the mesoscale flow (MTF), in units of terawatts per kilometer (TW km^{-1}), zonally low-passed using a wavelength equal to twice the large-scale/mesoscale threshold wavelength at each latitude. Fluxes shown in the (a) Atlantic, (b) Indo-Pacific, and (c) Southern Ocean basins.

ridional MTF in a given location usually has the same sign as the LTF, indicating that the mesoscale reinforces or intensifies the impact of the time-mean large-scale circulation. However, there are a few notable exceptions where the mesoscale counteracts the time-mean LTF. The western boundary of the southern Indian Ocean has a poleward LTF but an equatorward MTF, implying compensation of the large-scale gyre heat transport by mesoscale circulations (Figure 7b). A similar compensation is evident in the East Australian Current near southeast Australia, and in the Labrador Sea at the western edge of the North Atlantic subpolar gyre (Figure 7a).

3.3 Contributions of stationary versus time-varying mesoscale structure

As with the total temperature flux, the time-mean MTF may contain contributions from the time-mean v and T, as well as time-varying v and T

$$\overline{\mathrm{MTF}} = \overline{\mathrm{MTF}_{\mathrm{stat}}} + \overline{\mathrm{MTF}_{\mathrm{vary}}} \tag{7}$$

$$\overline{\mathrm{MTF}_{\mathrm{stat}}} = \overline{v_L}\,\overline{T_M} + \overline{v_M}\,\overline{T_L} + \overline{v_M}\,\overline{T_M} \tag{8}$$

$$\overline{\mathrm{MTF}_{\mathrm{vary}}} = \overline{v'_L T'_M} + \overline{v'_M T'_L} + \overline{v'_M T'_M} \tag{9}$$

with $^{-}$ indicating a time average. The stationary part of the contribution $\mathrm{MTF}_{\mathrm{stat}}$ can be explained in terms of time averages of the v and T components, while the time-varying part $\mathrm{MTF}_{\mathrm{vary}}$ is associated with rectified fluxes from transient motions (e.g., instability-generated eddies).

Figure 8 considers the contributions from stationary features relative to the time-varying flux at certain latitudes in the Indo-Pacific where the MTF is relatively large (Figure 4c). All of the mid-latitude and tropical transects in Figure 8 have western boundary currents (WBCs). These currents contribute to a peak in v_L near the coast, as well as an intensified boundary current jet and flanking recirculation just to the east that is shown in v_M (Figure 8, left column). These jet-recirculation pairs are mesoscale structures, since the core of the jet and the recirculation flow in opposite directions and are separated by only 2°-3° longitude. By integrating the MTF across each transect from west to east (Figure 8, right column), it can be seen that the stationary MTF contributions are associated with western boundaries: namely in the western Pacific at 32°N, 4°N, and 13°S, and the western Indian at 32°S. Furthermore, while 4°N and 13°S have larger contributions from time-varying mesoscale dynamics $\mathrm{MTF}_{\mathrm{vary}}$, it is the stationary structures $\mathrm{MTF}_{\mathrm{stat}}$ that contribute most to MTF at the mid-latitude transects.

If stationary mesoscale contributions to MHT are substantial, especially at mid-latitudes, then it is important to understand the velocity and temperature structure that contributes to the flux. The stationary MTFs near mid-latitude western boundaries are driven by a temperature difference between the poleward WBC jet and the equatorward recirculation (Figure 9). In the Gulf Stream, Kuroshio, and Brazil Current poleward of ~30° latitude, the poleward jet is associated with a local maximum in temperature due to the advection of waters from lower latitudes (Figure 9a-c). As a result, the water in the jet is warmer than the water in the recirculation, and the net MTF is poleward (Figure 7a-b). In contrast, the jet of the Agulhas is coincident with a steep gradient in temperature without a local maximum in temperature (Figure 9d); hence the water in the jet is cooler than in the recirculation and the net MTF is equatorward. The sign of the MTF associated with WBCs therefore depends on whether the local temperature profile is determined more by the temperature advection of the WBC jet (poleward MTF), or the frontal gradient that the WBC is aligned with (equatorward MTF). Most WBCs have both characteristics, but the degree to which one is dominant can be the difference between a stationary flux that is 0.12 PW poleward (Figure 8c) and 0.16 PW equatorward (Figure 8l).
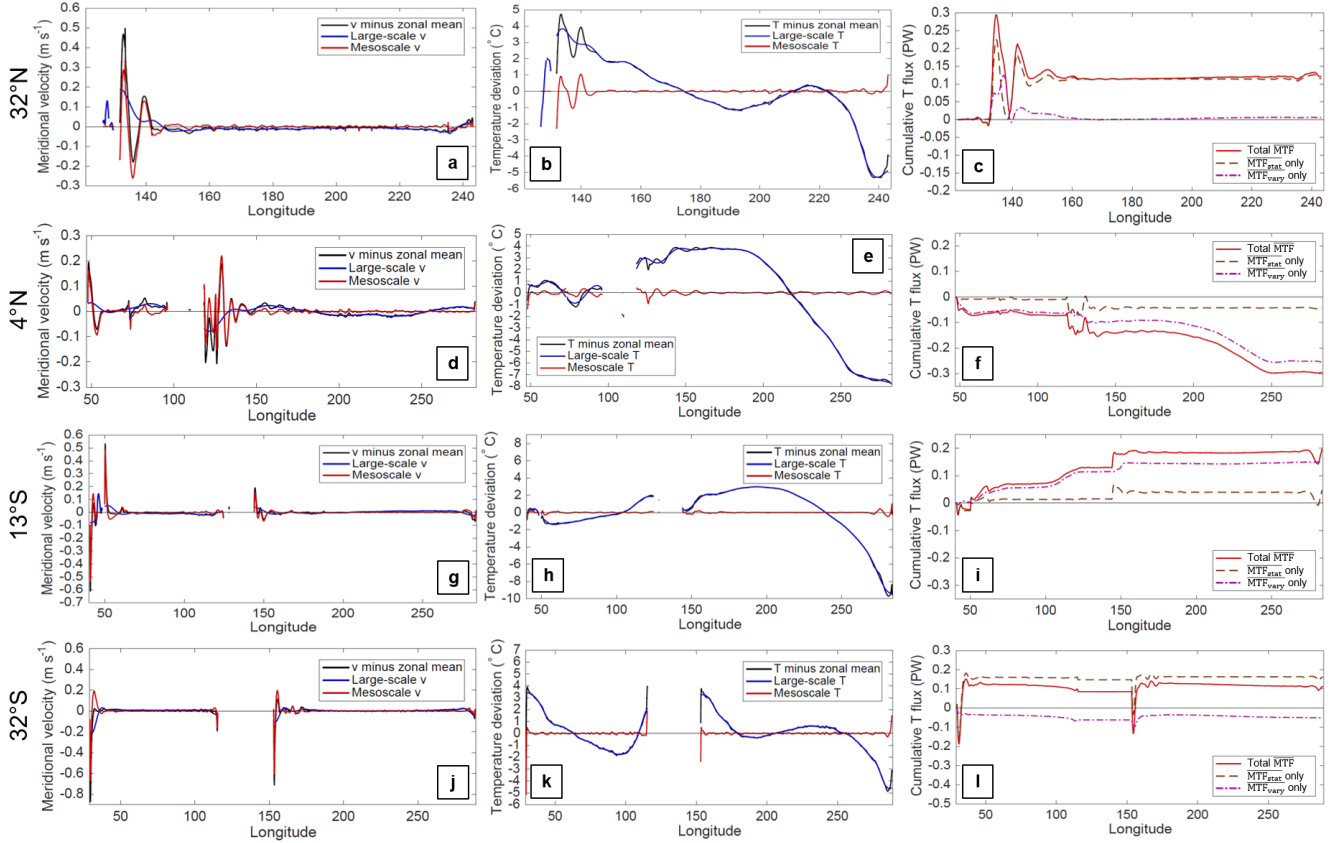
Figure 8. Left column: Decomposition of the time-mean meridional velocity at 95 m depth into large-scale v_L and mesoscale v_M in the Indo-Pacific basin, along latitude transects specified at left. Center column: Same but for the decomposition of time-mean temperature into T_L and T_M. Right column: The time-mean full-depth mesoscale temperature flux, cumulatively integrated from west to east, showing the total $\overline{\mathrm{MTF}}$, $\overline{\mathrm{MTF}_{\mathrm{stat}}}$, and $\overline{\mathrm{MTF}_{\mathrm{vary}}}$.

4 Difference between spatial and temporal flux decompositions

245 By targeting mesoscale spatial scales, our approach differs from methods that quantify "eddy" contributions to MHT based on temporal deviations in v and T. The temporal decomposition defines the "eddy" v' and T' as deviations from the time mean (e.g., $v = \bar{v} + v'$), and the contributions to MHT are given by

$$\int \overline{vT}\,dx = \int \left(\bar{v}\bar{T} + \overline{v'T'} \right) dx \tag{10}$$

and the second term on the right-hand side is the eddy contribution. Most commonly, the time mean is computed over the
250 entire period of record (which in this study would be the 32 years of model output). An alternative approach (Volkov et al.,
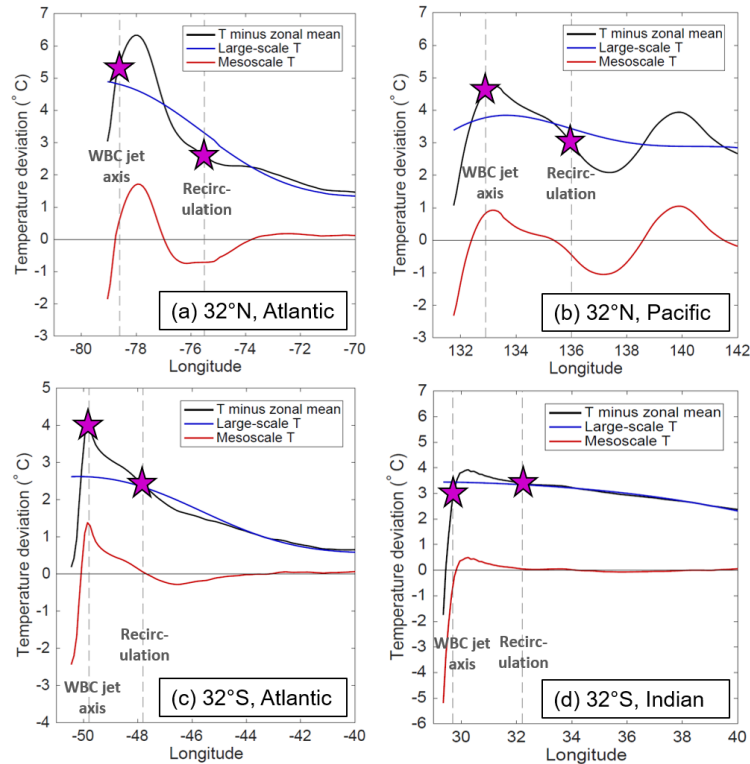
Figure 9. Temperature profiles at 95 m depth near the western boundary in the specified latitude and basin. The vertical gray dashed lines indicate the locations of peak velocities associated with the poleward western boundary current (WBC) jet, and the equatorward recirculation. The difference in temperature between these two locations (magenta stars) provides an indication of the mesoscale temperature flux from the jet and recirculation.

2008) computes the eddy term as the deviation from 3-month time means, so that the eddy contribution includes intraseasonal variations, but not seasonal or interannual variations. In this study, the mesoscale contribution to MHT using our method is compared to both definitions of the temporal eddy contribution, which are called the "time-varying" and "high frequency" components respectively.

255   Regarding contributions to the time-mean MHT, neither the time-varying nor high frequency components are uniformly consistent with the mesoscale contribution (Figure 10). Generally, the mesoscale MHT is closer to the high frequency contribution at low latitudes, and closer to the time-varying contribution at mid latitudes. One possible inference from this is that mesoscale dynamics tend to have consistently high frequencies in the tropics (where planetary wave and eddy propagation speeds are higher), while mesoscale dynamics at higher latitudes tend to propagate more slowly and take on lower frequencies.

260   The difference between time-varying and mesoscale MHT close to the equator may also be associated with the impact of long
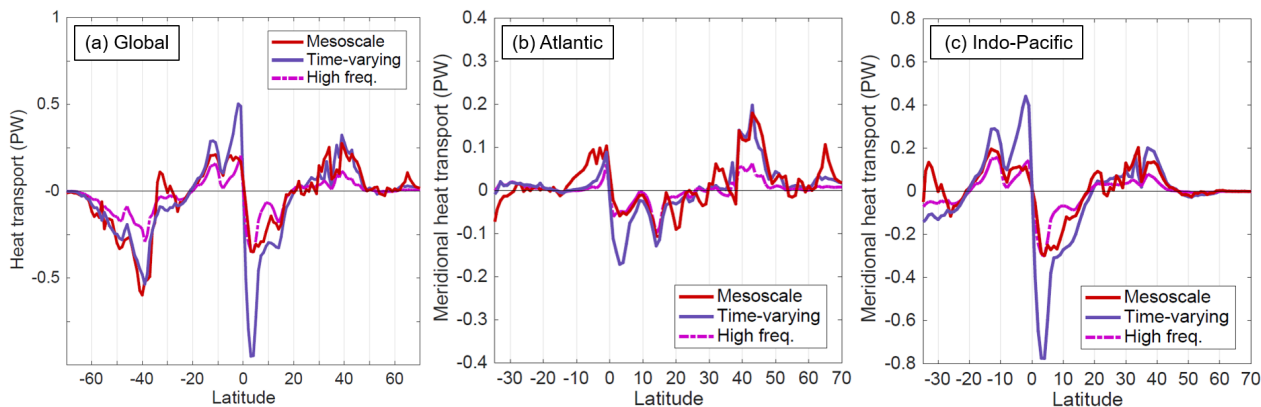
Figure 10. Comparison of various "eddy" formulations of the meridional heat transport as a function of latitude (a) globally, and in the (b) Atlantic and (c) Indo-Pacific. The three formulations are the mesoscale component, the time-varying component $v'T'$, and the high frequency component computed from v' and T' on timescales shorter than 3 months.

Kelvin and Rossby waves, which are both large-scale and time variable. Hence time-varying and high frequency MHT may include the impacts of large-scale variability that have very different dynamics from mesoscale eddies.
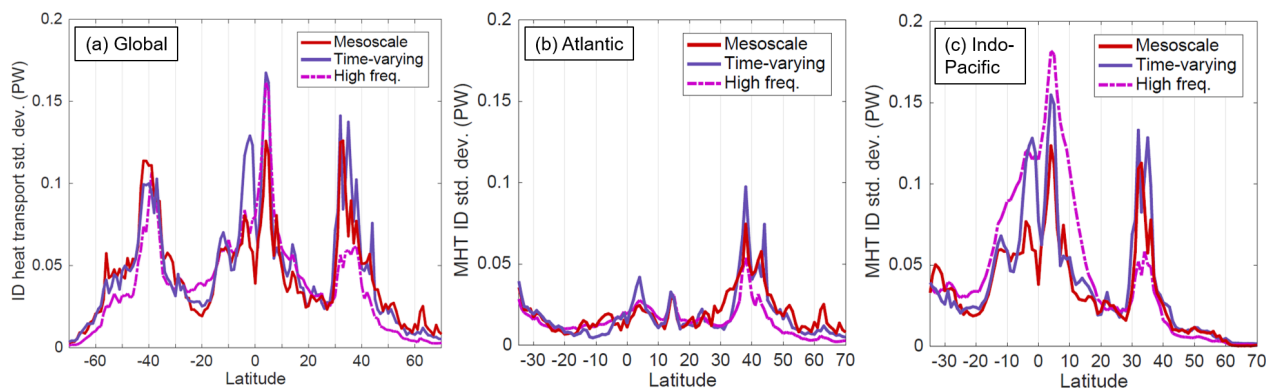
Figure 11. Interannual/decadal (ID) standard deviation of the spatial and temporal "eddy" formulations (a) globally and in the (b) Atlantic and (c) Indo-Pacific basins.

A comparison of the standard deviation associated with the ID time series of the three components (Figure 11) shows that all three components have spikes in temporal variability in the mid-latitudes and near the equator. As with the contributions to time-mean MHT, the ID variability of the mesoscale contribution more closely resembles the time-varying contribution at mid-
265 latitudes. In the tropics, the ID variability of the mesoscale does not resemble either component; in the tropical Indo-Pacific

the high frequency and time-varying standard deviations are both larger than the mesoscale, implying substantial contributions from large-scale ID variability.

5 Mesoscale interannual/decadal variability

270 ## 5.1 Locations of substantial mesoscale contributions
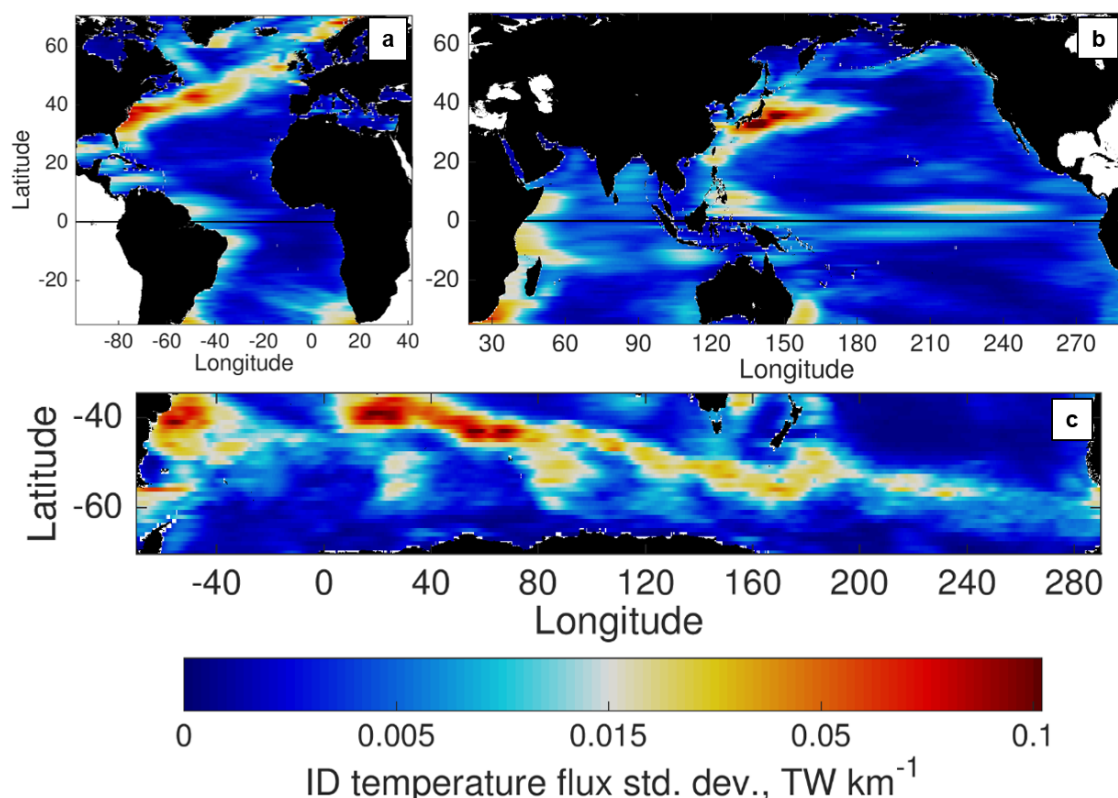
Figure 12. Standard deviation of the interannually-varying meridional temperature flux associated with the mesoscale flow, zonally smoothed. The "interannually-varying" flux is low-passed for periods >14 months prior to the computation of the standard deviation. Fluxes shown in the (a) Atlantic, (b) Indo-Pacific, and (c) Southern Ocean basins.

Mesoscale dynamics influence not only the time-mean MHT but also its variability on ID timescales (Figure 5), motivating a study of the regions where the mesoscale contributions to ID temperature flux variability are greatest. As with the time-mean MTF, the interannual and decadal variability of the MTF is mostly concentrated near western boundaries, the ACC, and the north equatorial Pacific and southern tropical Indian oceans (Figure 12). High levels of ID variability of the MTF also generally

275 coincide with regions of high EKE in the POP model simulation (Figure 1b). Notably, the subtropical eddy bands in the Pacific

and Indian Oceans seem to have a negligible impact on MTF ID variability. The POP model does underestimate EKE in these eddy bands relative to altimetry (Figure 1), but it still shows these bands as regions of elevated EKE; in contrast there is almost no elevation in ID MTF variability associated with these eddy bands. This indicates that mesoscale fluxes are not be particularly efficient at moving heat meridionally in subtropical eddy bands, at least in the POP simulation.
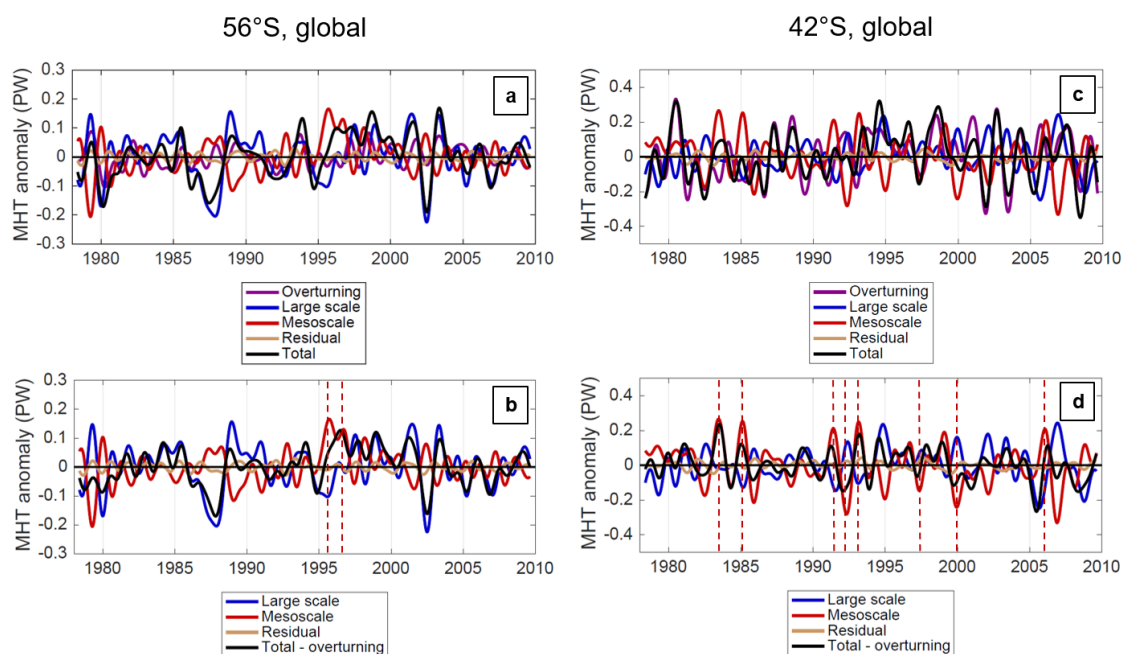
Figure 13. Time series of spatial components of MHT variability in the Southern Ocean across (a)-(b) 56°S and (c)-(d) 42°S, with time means removed. The top row shows all spatial components; the bottom row has the overturning component removed. The dashed vertical red lines in (b) and (d) indicate episodes where mesoscale MHT drives variations in the total non-overturning MHT.

280   Time series at specific latitudes can provide context for the contributions of MTFs relative to overturning and large-scale temperature fluxes. In the Southern Ocean, peaks in basin-integrated MTF ID variability occur at 56°S and 42°S (Figure 5a), but the role of the MTF is very different. At 56°S, the large-scale temperature flux is the driving component of ID MHT variability, with the mesoscale compensating (counteracting) the large-scale contributions to some extent (Figure 13a-b). One exception is the 1995–96 episode, when a positive (northward) mesoscale MHT anomaly pushes the total MHT at 56°S despite

285   a negative large-scale MHT anomaly. In contrast, at 42°S numerous extrema in the total MHT anomaly can be attributed to the mesoscale component (Figure 13d). This latitude is near the largest mesoscale contribution to time-mean MHT as well (at 40°S), indicating the impact of mesoscale dynamics on both the MHT steady state and ID variations in the Southern Hemisphere mid-latitudes.
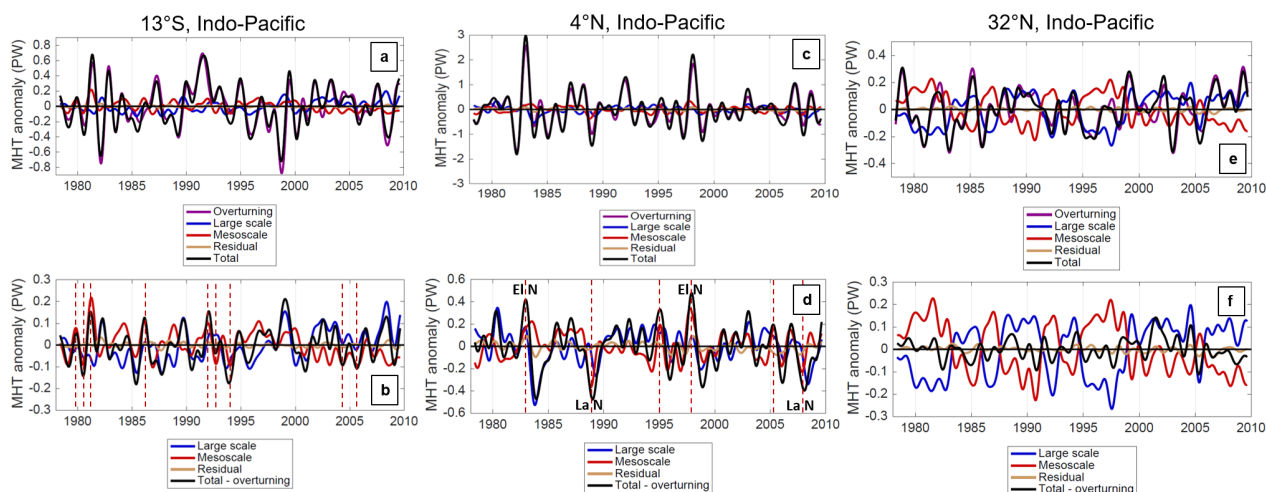
Figure 14. Time series of spatial components of MHT variability in the Indo-Pacific basin across (a)-(b) 13°S, (c)-(d) 4°N, and (e)-(f) 32°N, with time means removed. The top row shows all spatial components; the bottom row has the overturning component removed. The dashed vertical red lines in (b) and (d) indicate episodes where mesoscale MHT drives variations in the total non-overturning MHT. In panel (d) some major El Niño (El N) and La Niña (La N) events coincident with mesoscale extrema are also annotated.

Despite the overall dominance of the overturning circulation in MHT variability at low latitudes, mesoscale contributions are
290 still substantial at certain latitudes. Most of these contributions are in the Indo-Pacific, where local maxima in mesoscale MHT variability are located at 13°S, 4°S, and 4°N (Figures 5c, 12). With the overturning removed, the mesoscale contributions to ID MHT variability are quite apparent in the time series at 13°S and 4°N (Figures 14b,d). At 4°N many of these mesoscale extrema coincide with El Niño or La Niña events, likely due to the TIW activity across much of the Pacific at this latitude. The MTF variability is larger in the Pacific at 4°N than at 4°S (Figure 12), consistent with the larger EKE north of the equator
295 (Figure 1). In contrast, the ID MTF variability in the mid-latitude Pacific at 32°N largely acts to compensate the large-scale fluxes, leaving overturning MHT to drive total MHT variability (Figure 14e,f).

One more area of substantial ID MHT variability is in the North Atlantic, where large MTF variability is found extending across the ocean from the Gulf Stream near the southeast U.S. coast, to the North Atlantic Current near the British Isles (Figure 12). At 43°N in the Atlantic, where the amplitude of ID MHT variability is nearly equal between the three components, a
300 number of total MHT extrema can be attributed to the mesoscale component (Figure 15b). Elevated variability is also found further north near the coasts of Greenland and Norway (Figure 12). At 63°N the overturning component no longer influences MHT variability substantially, but large-scale and mesoscale fluxes both contribute to the total MHT time series (Figure 15d).
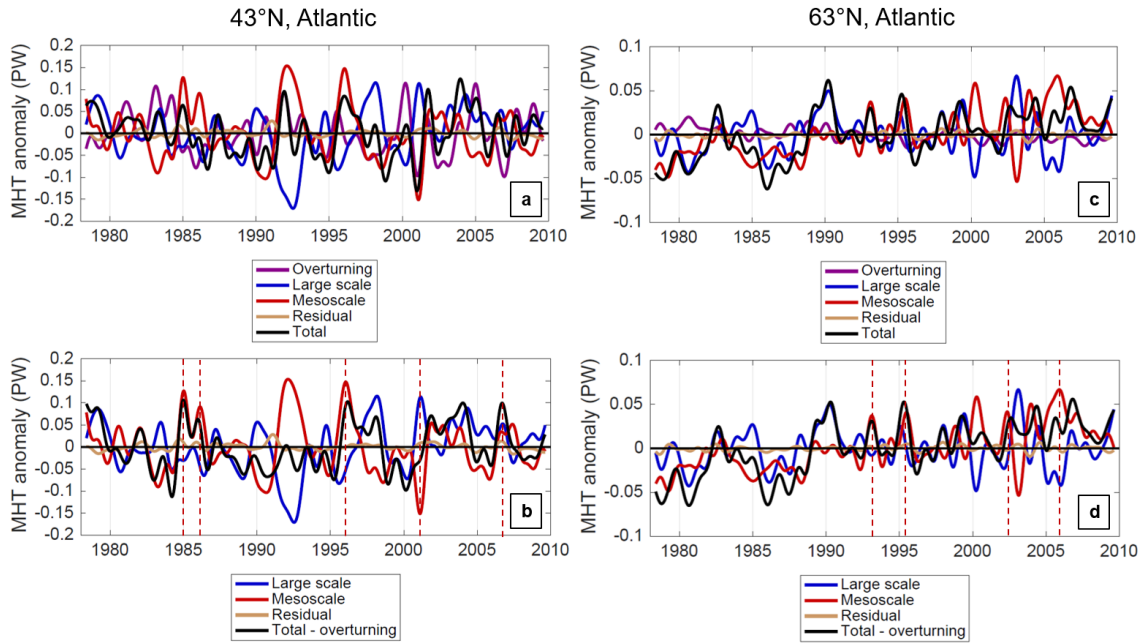
Figure 15. Time series of spatial components of MHT variability in the Atlantic Ocean across (a)-(b) 43°N and (c)-(d) 63°N, with the time means removed. The top row shows all spatial components; the bottom row has the overturning component removed. The dashed vertical red lines in (b) and (d) indicate episodes where mesoscale MHT drives variations in the total non-overturning MHT.

Another way to assess the contributions of MTF variability to basin-integrated MHT on ID timescales is to compute a linear regression or correlation between (1) the time series of MHT integrated across the basin at each latitude and (2) the local zonally-smoothed MTF time series along the transect. This regression-based flux contribution can be expressed as

$$R_{\mathrm{MTF}} = R_{\frac{\mathrm{loc}}{\mathrm{tot}}}\,\sigma_{\mathrm{tot}} = C(\mathrm{loc},\mathrm{tot})\sigma_{\mathrm{loc}} \tag{11}$$

where $R_{\frac{\mathrm{loc}}{\mathrm{tot}}}$ is the linear regression coefficient of the local MTF given the time series of the total basin-integrated temperature flux, σ_{loc} and σ_{tot} are the standard deviations of the local and total basin-integrated time series respectively, and $C(\mathrm{loc},\mathrm{tot})$ is the correlation coefficient of the local and total basin-integrated time series. The regression flux contribution R_{MTF} is the local temperature flux that would be expected to contribute to a basin-integrated value of 1 standard deviation above the mean; positive (negative) values of R_{MTF} indicate a positive (negative) correlation of the two time series. R_{MTF} can be expressed in units of temperature flux or heat flux, and the latter are used here. A similar analysis was shown in Figures 7-8 of Delman and Lee (2020) in profiles of longitude-depth, but MTFs are mostly vertically coherent, so here the "local" time series are depth-integrated.
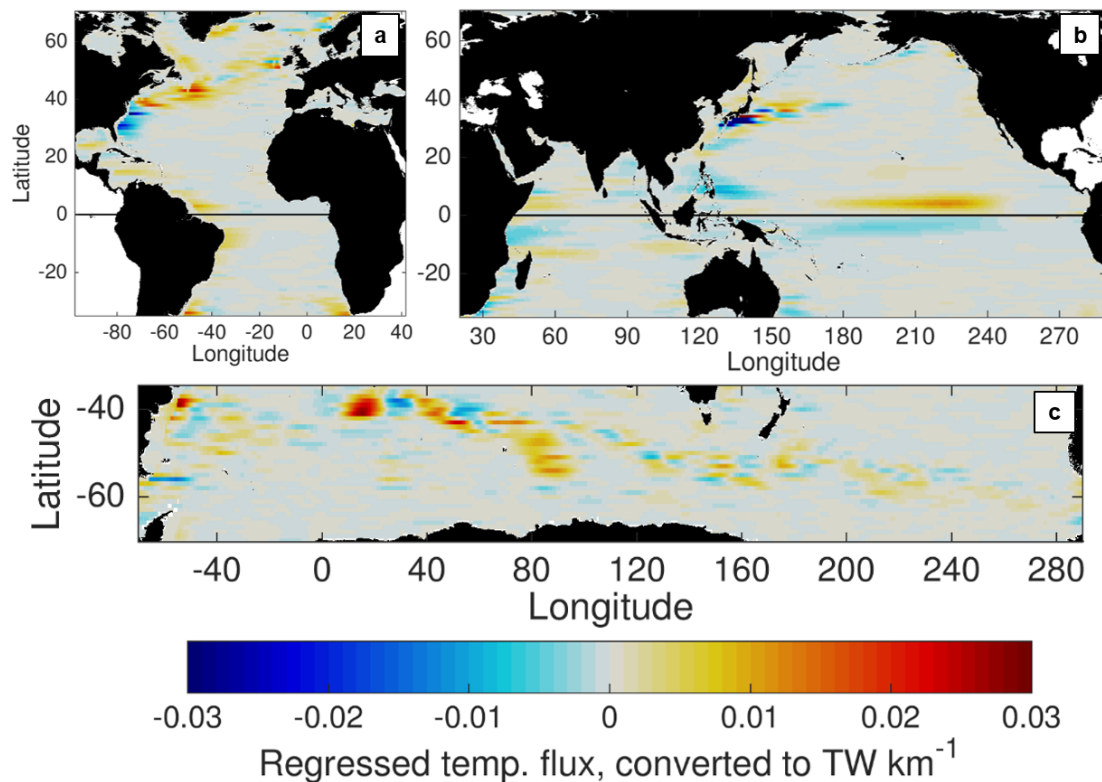
Figure 16. Local (zonally-smoothed) mesoscale temperature flux R_{MTF} that contributes to the total MHT variability on ID timescales, computed by linear regression at each latitude and basin. Positive values indicate that the MTF is positively correlated with (contributes to) total ID MHT variability; negative values indicate that the MTF is negatively correlated with (compensates) total ID MHT variability.

315   In Figure 16, R_{MTF} is computed such that the local time series is the MTF and the total time series is the total MHT (sum of all components) at ID timescales with the mean and seasonal cycle removed. These maps show the regions where local MTF has substantial variability that is coherent with total MHT variability in a given basin. Overall, three areas emerge where the MTF variability contributes substantially (and positively) to basin-integrated MHT variability: the North Atlantic, the tropical Indo-Pacific, and the Southern Ocean between 0°-100°E. In the North Atlantic, the positive contributions peak

320   at ~43°N, where the Grand Banks of Newfoundland protrude into the North Atlantic Current (Figure 16a). In contrast, the "negative" contributions of the Gulf Stream and the Kuroshio south of their separations from the continental shelf imply that MTF variations compensate other components (specifically large-scale temperature fluxes) and therefore decrease MHT variability on ID timescales at these latitudes. The tropical Indo-Pacific contributions are highest in the TIW bands (Figure 16b), with a notable asymmetry across the equator: north of the equator the MTF contributes directly to MHT variability,

325   while south of the equator the MTF compensates MHT variability from other components. The mesoscale contributions near

13°S (Figure 14a,b) are focused in the Indian Ocean on both the western and eastern sides, though they are weaker than the near-equatorial contributions. In the Southern Ocean, the Agulhas Return Current and lee of the Kerguelen Plateau emerge as hotspots for mesoscale contributions to total MHT (Figure 16c). The largest concentrations of MTF contribution are focused near the Agulhas Retroflection (45°-40°S, 10°-20°E), and just east of Kerguelen (55°-45°S, 70°-100°E).

330 ## 5.2 Surface EKE as a proxy for ID MTF variability

Local velocity variability and EKE have been considered in previous studies as possible observational proxies for lateral heat fluxes induced by mesoscale eddies (e.g., Stammer, 1998; Bolton et al., 2019; Müller and Melnichenko, 2020). Delman and Lee (2020) explored the degree to which variations in surface EKE can account for MTF variability at ID timescales, along the 40°N transect in the North Atlantic. By applying mixing length theory (e.g., Green, 1970; Holloway, 1986; Stammer, 1998)
335 the relationship can be expressed as

$$\mathrm{MTF} \approx \kappa \frac{\partial T}{\partial y} \tag{12}$$

$$\kappa \propto -\sqrt{v'^2} L_{\mathrm{mix}} \approx -\sqrt{\mathrm{EKE}} L_{\mathrm{mix}} \tag{13}$$

where κ is the diffusivity (which is generally negative or downgradient), and L_{mix} is the mixing length. According to this
340 construct, if the mixing length and meridional temperature gradient do not vary greatly, EKE should be correlated locally with the MTF.

Figure 17 shows the fraction of MTF variance at ID timescales explained by local variations in the surface EKE; the fraction of variance is equivalent to the squared correlation coefficient of the surface EKE and MTF. Many regions in the ocean have a significant correlation and fraction of variance explained. These areas include the southern excursions of the ACC, the
345 subtropical bands of eddy activity in the Indo-Pacific at ∼20°-25° latitude in both hemispheres, and the fringes of energetic western boundary currents. One characteristic shared by these areas is that they tend to have modest levels of time-mean EKE overall (Figure 1); in fact, many of these areas occur near the time-mean contour of 100 cm^2 s^{-2} in the POP model, which often separates energetic and quiescent regions in the ocean. However, in the core of more energetic regions with high EKE, surface EKE is not a good proxy for the MTF. These energetic regions include the Gulf Stream and Kuroshio extensions as
350 well as the Agulhas Return Current, which are annotated in Figure 17. The lack of significant MTF variance associated with EKE in these high-energy regions may be attributed to several factors. EKE is a convenient and widely-understood metric of mesoscale activity, but it is based on removing a temporal mean from the velocity field and it is not the most precise way to gauge the level of mesoscale energy present. Higher levels of EKE may be associated with an anomalous placement of the current jet and associated front, which does not necessarily change the cross-jet flux. Moreover, strong velocity jets tend to
355 suppress diffusivity across fronts by reducing the mixing length (Ferrari and Nikurashin, 2010); hence variations of the mixing
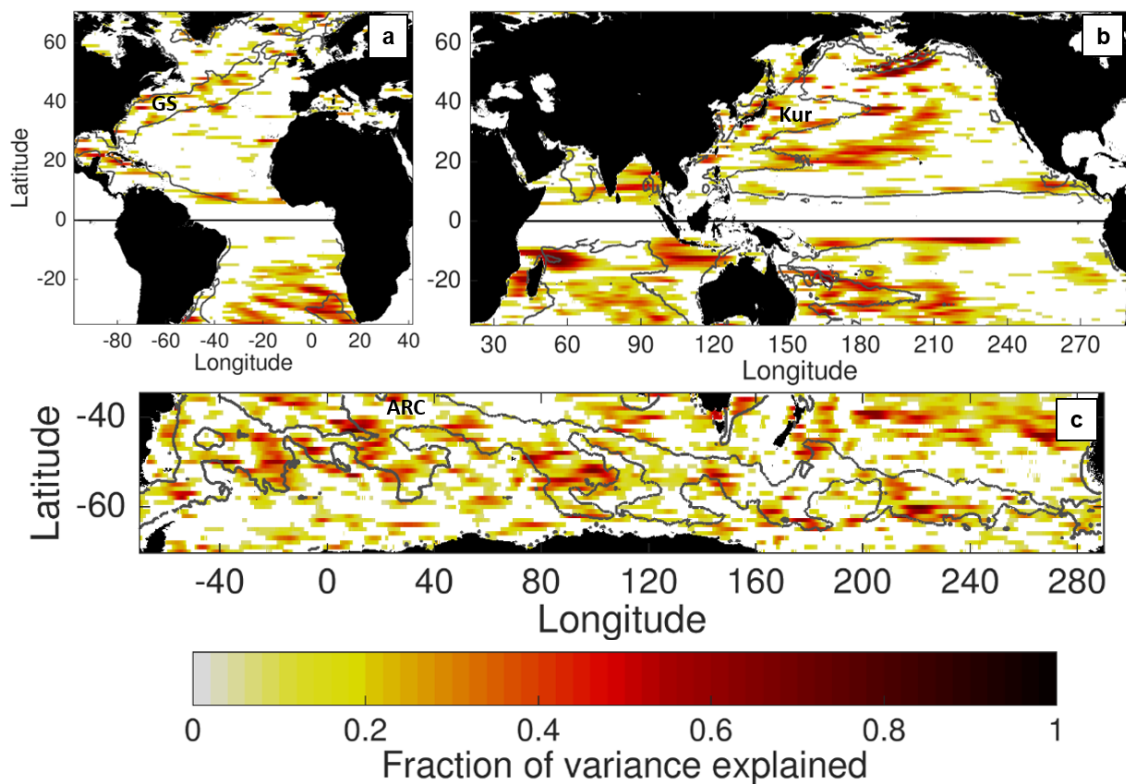
Figure 17. Fraction of zonally-smoothed mesoscale temperature flux variance explained by the regression onto surface EKE, at ID timescales. Only areas with a signal-to-noise ratio > 1 at the 95% confidence level are shaded. The gray contour indicates 100 cm^2 s^{-2} time-mean EKE in the POP model. Several regions (GS, Kur, ARC) with very high time-mean EKE are labeled.

length unrelated to EKE interfere with the relationship between EKE and cross-frontal fluxes. Ultimately the MTF depends not only on the mesoscale velocity and temperature variance, but on the local correlation between v_M and T_M (Delman and Lee, 2020), and the factors affecting this correlation need to be further explored.

6   Conclusions

360   This analysis uses the method first applied in Delman and Lee (2020) in the North Atlantic to quantify mesoscale temperature fluxes in the global oceans, and their contribution to the time-mean and ID variability of MHT. The resulting assessment indicates that mesoscale ocean dynamics generally spread heat outward from the subtropics: poleward in mid-latitudes, and equatorward in the tropics. Hence the net effect of the mesoscale MHT is to flux heat from where thermocline isotherms are deepest (in subtropical gyres) to where they are shallower, consistent with the "slumping" associated with typical parameteri-

365   zations of mesoscale effects in models (e.g., Gent and McWilliams, 1990). Despite this, mesoscale temperature fluxes do not

always act to diminish large-scale horizontal temperature gradients. In the Agulhas and East Australian Current, mesoscale recirculations act to flux heat equatorward at mid-latitudes (Figure 7b), such that the net mesoscale MHT is equatorward at 35°-30°S in the Indo-Pacific (Figure 4c). Moreover, the time variability of mesoscale temperature fluxes on ID timescales is not well explained by surface EKE variability in the most energetic regions of the ocean; hence a more nuanced understanding
370 of how mesoscale processes flux heat across strong currents is needed.

It is important to highlight the differences between the definition of the mesoscale flux described here and the "eddy" fluxes used in other studies. While eddy fluxes are typically associated with deviations from a zonal or temporal mean, neither of these definitions separates the effects of mesoscale phenomena from those of basin scale gyres or long planetary waves. Moreover, stationary mesoscale recirculations contribute substantially to mesoscale MHT (Figure 8, right column). The effects
375 of these recirculations are not included in an eddy flux based on temporally-varying flow, but these recirculations still need to be parameterized as they will not be accurately simulated in a coarse-resolution (∼1° grid spacing) ocean model. Since spatial rather than temporal resolution is often the limiting factor in simulating ocean dynamics, flux diagnostics based on spatial scales are needed to improve model parameterizations as well as to compare mesoscale-permitting model simulations.

The scope of this study leaves a number of questions unanswered about the effects of mesoscale dynamics on heat pathways
380 through the ocean. The large-scale/mesoscale decomposition used in this study is applied only in one dimension (zonally), and therefore does not separate divergent from rotational fluxes. Only the divergent fluxes contribute to changes in ocean heat content locally, so a separation of the large-scale and mesoscale in both horizontal dimensions is needed to compute the divergence and assess the impact of mesoscale dynamics on local heat content. The relationship between MTF variability and other characteristics of the large-scale and mesoscale state also needs to be investigated more extensively. The disconnect
385 between surface EKE and MTF variability in the most active mesoscale regions may be the result of factors such as variability in large-scale temperature gradients, mixing length, and the local geometry of the mesoscale flow field. Assessing the influence of these factors on MTF variability, perhaps with the aid of more complex statistics and/or deep learning techniques (George et al., 2019), can be expected to produce improvements in model parameterizations and better predictive models for tracer fluxes across mesoscale fronts.

390 *Data availability.* The POP model output used in this study is stored on NCAR's High Performance Storage System (HPSS); the full model output in 5-day averages is available with a user account (through https://www2.cisl.ucar.edu) by logging into cheyenne.ucar.edu and accessing the following path on HPSS: /home/bryan/johnsonb/g.e01.GIAF.T62_t12.003/ocn/hist/. Source code to run the POP2 model is available at http://www.cesm.ucar.edu/models/cesm1.0/pop2/. The CMEMS surface dynamic topography data used to produce the analysis in Figure 1 are available from http://marine.copernicus.eu/services-portfolio/access-to-products/ by searching for the Product ID
395 SEALEVEL_GLO_PHY_L4_REP_OBSERVATIONS_008_047.

Author contributions. Primary author Andrew Delman wrote the code, carried out the analysis presented, and drafted the manuscript. Tong Lee supervised the project, providing input into the direction of the research and edits to the manuscript.

Acknowledgements. The research was carried out at the Jet Propulsion Laboratory, California Institute of Technology, under a contract
400 with the National Aeronautics and Space Administration (80NM0018D004) with the support of NASA Physical Oceanography. The authors
would like to acknowledge Benjamin Johnson who ran the POP model configuration and made the output available, as well as Frank Bryan
at the National Center for Atmospheric Research who helped us obtain the output.

References

Abernathey, R. and Haller, G.: Transport by Lagrangian vortices in the eastern Pacific, Journal of Physical Oceanography, 48, 667–685, 2018.

405   Bolton, T., Abernathey, R., and Zanna, L.: Regional and temporal variability of lateral mixing in the North Atlantic, Journal of Physical Oceanography, 49, 2601–2614, 2019.

Bryan, K.: Poleward heat transport by the ocean: observations and models, Annual Review of Earth and Planetary Sciences, 10, 15–38, 1982.

Chaigneau, A. and Pizarro, O.: Eddy characteristics in the eastern South Pacific, Journal of Geophysical Research: Oceans, 110, 2005.

Charney, J. G. and Stern, M.: On the stability of internal baroclinic jets in a rotating atmosphere, Journal of the Atmospheric Sciences, 19,

410   159–172, 1962.

Chelton, D. B., Schlax, M. G., and Samelson, R. M.: Global observations of nonlinear mesoscale eddies, Prog. Oceanog., 91, 167–216, 2011.

Computational and Information Systems Laboratory: Yellowstone: IBM iDataPlex System (University Community Computing), Boulder, CO: National Center for Atmospheric Research. http://n2t.net/ark:/85065/d7wd3xhc., 2016.

Cox, M. D.: An eddy resolving numerical model of the ventilated thermocline, Journal of Physical Oceanography, 15, 1312–1324, 1985.

415   Delman, A. and Lee, T.: A new method to assess mesoscale contributions to meridional heat transport in the North Atlantic Ocean, Ocean Science, 16, 979–995, 2020.

Delman, A. S., McClean, J. L., Sprintall, J., Talley, L. D., and Bryan, F. O.: Process-specific contributions to anomalous Java mixed layer cooling during positive IOD events, Journal of Geophysical Research: Oceans, 123, 4153–4176, 2018.

Dong, C., McWilliams, J. C., Liu, Y., and Chen, D.: Global heat and salt transports by eddy movement, Nature Communications, 5, 1–6,

420   2014.

Dong, D., Brandt, P., Chang, P., Schütte, F., Yang, X., Yan, J., and Zeng, J.: Mesoscale eddies in the northwestern Pacific Ocean: Three-dimensional eddy structures and heat/salt transports, Journal of Geophysical Research: Oceans, 122, 9795–9813, 2017.

Ducet, N., Traon, P. Y. L., and Reverdin, G.: Global high–resolution mapping of ocean circulation from TOPEX/Poseidon and ERS–1 and –2, J. Geophys. Res., 105, 19,477–19,498, 2000.

425   Eady, E. T.: Long waves and cyclone waves, Tellus, 1, 33–52, 1949.

Ferrari, R. and Nikurashin, M.: Suppression of eddy diffusivity across jets in the Southern Ocean, Journal of Physical Oceanography, 40, 1501–1519, 2010.

Gent, P. R. and McWilliams, J. C.: Isopycnal mixing in ocean circulation models, Journal of Physical Oceanography, 20, 150–155, 1990.

George, T., Manucharyan, G., and Thompson, A.: Deep learning to infer eddy heat fluxes from sea surface height patterns of mesoscale

430   turbulence, 2019.

Greatbatch, R., Zhai, X., Claus, M., Czeschel, L., and Rath, W.: Transport driven by eddy momentum fluxes in the Gulf Stream Extension region, Geophysical Research Letters, 37, 2010.

Green, J.: Transfer properties of the large-scale eddies and the general circulation of the atmosphere, Quarterly Journal of the Royal Meteorological Society, 96, 157–185, 1970.

435   Griffies, S. M., Winton, M., Anderson, W. G., Benson, R., Delworth, T. L., Dufour, C. O., Dunne, J. P., Goddard, P., Morrison, A. K., Rosati, A., et al.: Impacts on ocean heat from transient mesoscale eddies in a hierarchy of climate models, Journal of Climate, 28, 952–977, 2015.

Hausmann, U. and Czaja, A.: The observed signature of mesoscale eddies in sea surface temperature and the associated heat transport, Deep Sea Research Part I: Oceanographic Research Papers, 70, 60–72, 2012.

Holloway, G.: Estimation of oceanic eddy transports from satellite altimetry, Nature, 323, 243–244, 1986.

440   Jayne, S. R. and Marotzke, J.: The oceanic eddy heat transport, Journal of Physical Oceanography, 32, 3328–3345, 2002.

Jochum, M. and Murtugudde, R.: Temperature advection by tropical instability waves, Journal of Physical Oceanography, 36, 592–605, 2006.

Johns, W. E., Baringer, M. O., Beal, L., Cunningham, S., Kanzow, T., Bryden, H. L., Hirschi, J., Marotzke, J., Meinen, C., Shaw, B., et al.:
    Continuous, array-based estimates of Atlantic Ocean heat transport at 26.5 N, Journal of Climate, 24, 2429–2449, 2011.

Johnson, B. K., Bryan, F. O., Grodsky, S. A., and Carton, J. A.: Climatological annual cycle of the salinity budgets of the subtropical maxima,
445   Journal of Physical Oceanography, 46, 2981–2994, 2016.

Large, W. G. and Yeager, S. G.: Diurnal and decadal global forcing for ocean and sea-ice models: the data sets and flux climatologies, NCAR
    Tech. Note. NCAR/TN-460+STR, 2004.

Large, W. G. and Yeager, S. G.: The climatology of an interannually–varying air sea flux data set, Clim. Dyn., 33, 341–364, 2009.

Laxenaire, R., Speich, S., Blanke, B., Chaigneau, A., Pegliasco, C., and Stegner, A.: Anticyclonic eddies connecting the western boundaries
450   of Indian and Atlantic oceans, Journal of Geophysical Research: Oceans, 123, 7651–7677, 2018.

Laxenaire, R., Speich, S., and Stegner, A.: Agulhas Ring Heat Content and Transport in the South Atlantic Estimated by Combining Satellite
    Altimetry and Argo Profiling Floats Data, Journal of Geophysical Research: Oceans, 125, e2019JC015 511, 2020.

Marshall, J. and Shutts, G.: A note on rotational and divergent eddy fluxes, Journal of Physical Oceanography, 11, 1677–1680, 1981.

Müller, V. and Melnichenko, O.: Decadal Changes of Meridional Eddy Heat Transport in the Subpolar North Atlantic Derived From Satellite
455   and In Situ Observations, Journal of Geophysical Research: Oceans, 125, e2020JC016 081, 2020.

Müller, V., Kieke, D., Myers, P. G., Pennelly, C., Steinfeldt, R., and Stendardo, I.: Heat and freshwater transport by mesoscale eddies in the
    southern subpolar North Atlantic, Journal of Geophysical Research: Oceans, 124, 5565–5585, 2019.

Smith, R., Jones, P., Briegleb, B., Bryan, F., Danabasoglu, G., Dennis, J., Dukowicz, J., Eden, C., Fox-Kemper, B., Gent, P., Hecht, M.,
    Jayne, S., Jochum, M., Large, W., Lindsay, K., Maltrud, M., Norton, N., Peacock, S., Vertenstein, M., and Yeager, S.: The Parallel Ocean
460   Program (POP) reference manual, Tech. Rep. LAUR-10-01853, Los Alamos National Laboratory, and National Center for Atmospheric
    Research, 2010.

Stammer, D.: On eddy characteristics, eddy transports, and mean flow properties, Journal of Physical Oceanography, 28, 727–739, 1998.

Sun, B., Liu, C., and Wang, F.: Global meridional eddy heat transport inferred from Argo and altimetry observations, Nature Scientific
    Reports, 9, 1–10, 2019.

465   Talley, L. D.: Shallow, intermediate, and deep overturning components of the global heat budget, Journal of Physical Oceanography, 33,
    530–560, 2003.

Ushakov, K. and Ibrayev, R.: Assessment of mean world ocean meridional heat transport characteristics by a high-resolution model, Russian
    Journal of Earth Sciences, 18, 2018.

Volkov, D. L., Lee, T., and Fu, L.-L.: Eddy-induced meridional heat transport in the ocean, Geophysical Research Letters, 35, 2008.

470   Zhao, J., Bower, A., Yang, J., Lin, X., and Holliday, N. P.: Meridional heat transport variability induced by mesoscale processes in the
    subpolar North Atlantic, Nature Communications, 9, 1–9, 2018.